Scanning Microscopy

Volume 7 | Number 3 Article 4

6-30-1993

Scanning Tunneling Microscopy: A Chemical Perspective

C. Julian Chen
T. J. Watson Research Center

Scanning Microscopy, Vol. 7, No. 3, 1993 (Pages 793-804) 0891-7035/93$5.00+.00
Scanning Microscopy International, Chicago (AMF O'Hare), IL 60666 USA

SCANNING TUNNELING MICROSCOPY: A CHEMICAL PERSPECTIVE

C. Julian Chen

IBM Research Division, T.J. Watson Research Center
P O Box 218, Yorktown Heights, NY 10598

Telephone number: 914 945 2935 / FAX number 914 945 2141

(received for publication December 16, 1992; and in revised form June 30, 1993)

Abstract

In this review article, scanning tunneling microscopy (STM) is presented in a chemical perspective. The typical distance from the nucleus of the apex atom of the tip to the top-layer nuclei of the sample is 4-6 Å, where a strong attractive atomic force, i.e., a partial covalent bond, arises between the tip and the sample. The origin of the covalent bond is the back-and-forth transfer of electrons between two atoms, which Pauling has called **resonance**. While a bias voltage is applied between them, a net electron current in a specific direction arises. This **tunneling** current is a result of the overlap of the tip electronic state and the sample electronic state, same as the chemical bond. The imaging process of STM can be considered as a sequence of local bond forming and bond rupturing. A quantitative understanding of the STM imaging mechanism can be achieved in such a chemical perspective. A natural consequence of this perspective is that the tip, partially bonded with the sample, can play an active role in local chemical reactions. The tip can either involve directly in a chemical reaction with the atoms on the sample surface or induce local chemical reactions on the sample surface as a local catalyst.

Key Words: Scanning tunneling microscopy, atomic force microscopy, chemical bond.

Introduction

Since John Dalton (1808) scientifically stated the hypothesis of atoms, the concept of atoms and the interactions between atoms have been the cornerstone of modern chemistry (Figure 1). Dalton proposed not only the concepts of atoms, but also the "adhesive force" between atoms which binds several atoms together to form molecules. Such an adhesive force is what later becomes the concept of the **chemical bond**. A universal form of the chemical bond is the **covalent bond**. According to Linus Pauling (1977), the **covalent bond** is formed by an electron oscillating between two fragments of the molecule, which he called **resonance**.

The concept of the chemical bond is microscopic in nature. However, up to very recent years, the knowledge about chemical bonds is derived from macroscopic measurements. The closest to a microscopic study of the interactions between atoms and molecules is the molecular beam experiment. Two beams of atoms or molecules, prepared with well-characterized quantum states, are allowed to cross each other in a vacuum chamber. The composition and electronic states of the outcome beams are then analyzed. To make an analogy, the scientist arranges two dancers to perform a ballet. Because of some practical limitation, he could not see what happens on the stage. After the ballet, he interviewed the dancers about their performance. Obviously, the after-the-stage information is very limited. The dancers may ask a logical question of why not watch their performance on the stage! For a ballet, to watch it on stage is simple. Visible light is a superb information medium. For individual atoms, the wavelength of the visible light is but too large. The X-ray photons are not sensitive to outer shell electrons which participate in chemical reactions. The question is, how to obtain information about two atoms during their encounter?

Let us imagine several possible ways to get information from two fragments of a molecule during their encounter. First, when the two atoms are in a short distance, an attractive force will occur. If the distance is

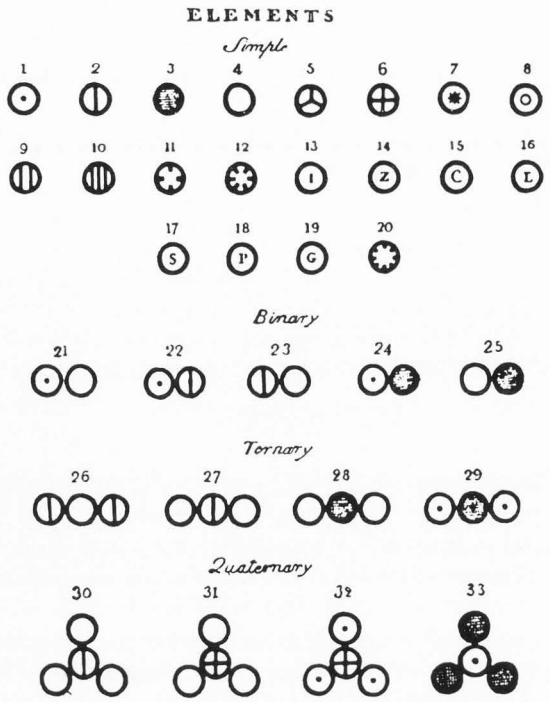

Figure 1. A chart in Dalton's book, published in 1808. In modern symbols, these atoms are: 1, H; 2, N; 3, C; 4, O; 5, P; 6, S; 7, Mg; 8, Ca; 9, Na; 10, K; 11, Sr; 12, Ba; 13, Fe; 14, Zn; 15, Cu; 16, Pb; 17, Ag; 18, Pt; 19, Au; 20, Hg. Dalton also proposed that the adhesion force between atoms can bring them together to form molecules.

---

too short, the repulsive force dominates. At larger distances, the weak van der Waals force occurs. At medium distances, the attractive force is the chemical bond, whose magnitude and dependence on the interatomic distance are of primary interest. To enable the force to be measured, certain force meter should be attached to the molecular fragments. In order to do this, each atom must be attached to a piece of solid, such that the force can be measured as the force between two pieces of solid. Obviously, at least one of the solid pieces must be of a shape of a tip to ensure that only the force between two molecular fragments is measured. On the other hand, the covalent bond, or according to Lewis, the **chemical bond**, is due to the **resonance**, or a continuous back-and-forth transfer of electrons between two atoms. The movement of electrons makes an electrical current. By attaching the two molecular fragments with two pieces of conductors, and applying a voltage between them, a net electrical current should be detected. This is the tunneling current. If the relative position of the two atoms can be controlled in a three-dimensional way, a complete knowledge about the interactions between the two molecular fragments can be obtained.

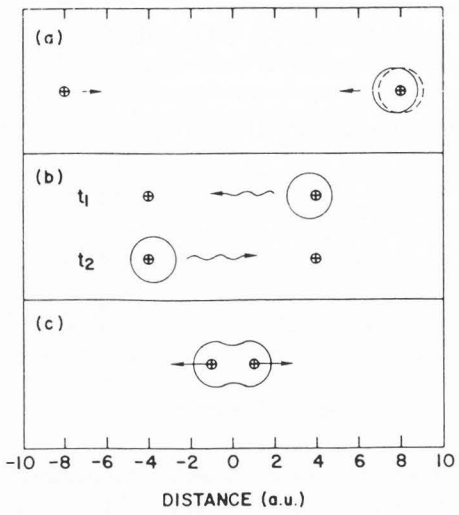

Figure 2. Three regimes of interaction in the hydrogen molecular ion. (**a**) At large distances, R > 16 a.u., the system can be considered as a neutral hydrogen atom plus a proton. The polarization of the hydrogen atom due to the field of the proton generates a van der Waals force. (**b**) At intermediate distances, 16 a.u. > R > 4 a.u., the electron can tunnel to the vicinity of another proton, and *vice versa*. A resonance force is generated, which is either attractive or repulsive. (**c**) At short distances, R < 4 a.u., proton-proton repulsion becomes important.

This scenario is but the essence of scanning tunneling microscopy (STM; Binnig and Rohrer, 1982, 1986) and atomic force microscopy (AFM; Binnig *et al.*, 1986). Such a view of STM and AFM can be characterized as a **chemical perspective** (Baratoff, 1984; Flores *et al*, 1988; Hamers, 1989; Ohnishi and Tsukada, 1989; Avouris, 1990; Chen, 1991a, 1991b, 1993).

Resonance and the Chemical Bond

The recognition of the relation between the chemical bond and electron tunneling is not new. Shortly after the discovery of quantum mechanics, Pauling suggested a theory of the chemical bond in terms of **resonance** (see Pauling, 1977). The concept of resonance and its relation to the chemical bond can be clearly illustrated by the example of the hydrogen molecular ion, the simplest of all molecules. If one tears a hydrogen molecular ion apart, it will become a neutral hydrogen atom plus a positive hydrogen ion (a proton). When a proton encounters with a neutral hydrogen atom, a chemical reaction occurs.

Figure 2 shows three regimes of interaction in a hydrogen molecular ion. At large distances, the system

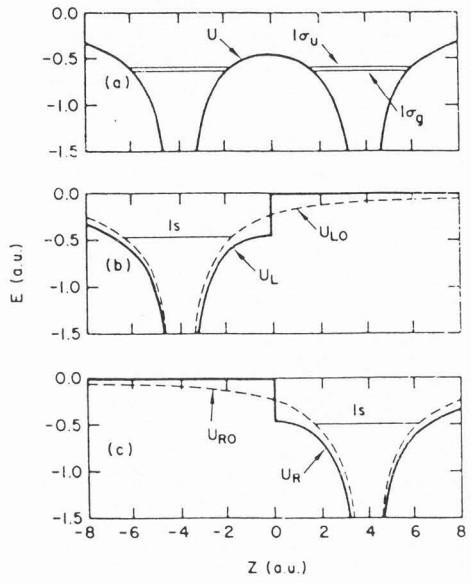

Figure 3. Perturbation treatment of the hydrogen molecular ion. (**a**) The exact potential curve and the exact energy levels of the problem. (**b**) Solid curve, the left-hand-side potential for a perturbation treatment; dotted curve, the potential for a free hydrogen atom. (**c**) Solid curve, the right-hand-side potential for a perturbation treatment; dotted curve, the potential for a free hydrogen atom.

---

can be considered as a neutral hydrogen atom plus a proton. The electrical field of the proton polarizes the hydrogen atom. As a result, a van der Waals force is induced. The van der Waals force dominates as the proton-proton distance R > 8 Å. At a distance R < 8 Å, the 1s electron at the vicinity of the right proton has an appreciable probability to tunnel into the 1s state of the left proton, and *vice versa*. In other words, at almost any time, the electron is shared by the two protons. This tunneling phenomenon gives rise to a **resonance** and results in a lowering of the total energy (Pauling, 1977). The resonance gives rise to a bonding state, with a lower total energy (attractive force); and an antibonding state, with a higher total energy (repulsive force). At even shorter distances, e.g., R < 2.5 Å, the repulsive force between the protons becomes important, and the net force becomes repulsive regardless of the type of the electronic states.

In the following, we discuss the three regimes in details.

van der Waals force

As shown in Figure 2, at large distances, the system can be considered as a neutral hydrogen atom plus an isolated proton with a polarization interaction (or van del Waals interaction) between them. The van der Waals force can be treated as a classical phenomenon by introducing a phenomenological polarizability α. In atomic units, the binding energy due to van del Waals force is (Landau and Lifshitz, 1977):

$$M = -\frac{2}{e} Re^{-R}. \tag{1}$$

Resonance energy

As shown in Figure 2, at a shorter proton-proton separation (R < 16 a.u. or R < 8 Å), the electron in the 1s state in the vicinity of one proton has an appreciable probability to tunnel to the 1s state in the vicinity of another proton. Naturally, this problem can be treated by a time-dependent Schrodinger's equation,

$$i\frac{\partial \Psi(\mathbf{r}, t)}{\partial t} = \left[-\frac{1}{2}\nabla^2 + U\right]\Psi(\mathbf{r}, t), \tag{2}$$

where U is the potential curve for the hydrogen molecule ion, as shown in Figure 3.

The concept of resonance can be understood from the point of view of time-dependent perturbation. First, we start by defining a pair of one-center potentials, U_L and U_R, and the corresponding right-hand-side states and the left-hand-side states, which are solutions of corresponding time-dependent Schrodinger's equations:

$$i\frac{\partial \Psi_L(\mathbf{r}, t)}{\partial t} = \left[-\frac{1}{2}\nabla^2 + U_L\right]\Psi_L(\mathbf{r}, t), \tag{3}$$

$$i\frac{\partial \Psi_R(\mathbf{r}, t)}{\partial t} = \left[-\frac{1}{2}\nabla^2 + U_R\right]\Psi_R(\mathbf{r}, t). \tag{4}$$

We denote the ground-state solutions of equation (3) and equation (4) as:

$$\Psi_L(\mathbf{r}, t) = \psi_L(\mathbf{r})e^{-iE_0 t}, \tag{5}$$

$$\Psi_R(\mathbf{r}, t) = \psi_R(\mathbf{r})e^{-iE_0 t}. \tag{6}$$

Now, we look for solutions of equation (2) which are linear combinations of the solutions of equation (3) and equation (4). In other words, we make the following *Ansatz*:

$$\Psi(\mathbf{r}, t) = a_L(t)\psi_L(\mathbf{r})e^{-iE_0 t} + a_R(t)\psi_R(\mathbf{r})e^{-iE_0 t}. \tag{7}$$

Substituting equation (7) into equation (2), one finds that the evolution of the coefficients satisfy the following equations:

$$\dot{a}_L(t) = iMa_R(t), \tag{8}$$

$$\dot{a}_R(t) = iMa_L(t). \tag{9}$$

The transition matrix element M, is exactly the modified

Bardeen integral in tunneling theory (see Chen, 1991b):

$$M = \frac{1}{2} \int [\psi_R \nabla \psi_L - \psi_L \nabla \psi_R] \bullet d\,\mathbf{S}, \qquad (10)$$

which is evaluated on the separation surface, i.e., the median plane (see Figure 3). For the hydrogen molecular ion, the result is (Holstein, 1955; Herring, 1962; Landau and Lifshitz, 1977):

$$M = -\frac{2}{e} R e^{-R}. \qquad (11)$$

A specific solution of equation (2) now depends on the initial condition. If at t = 0, the electron is in the left-hand-side state, the solution is:

$$\Psi_1(\mathbf{r}, t) = [\cos Mt\, \psi_L(\mathbf{r}) + i \sin Mt\, \psi_R(\mathbf{r})] e^{-iE_0 t} \qquad (12)$$

This solution describes a back-and-forth migration of the electron between the two protons. At t = 0, the electron is revolving about the left-hand-side proton with a frequency $f = |E_o|/h$. Then, the electron gradually migrates to the right hand side. At $t = \pi/|M|$, the electron has migrated entirely to the right-hand side; and at $t = 2\pi/|M|$, the electron comes back to the left-hand side, etc. In other words, the electron migrates back and forth between the two protons with a frequency $\nu = |M|/h$. Similarly, we have another solution:

$$\Psi_2(\mathbf{r}, t) = [\cos Mt\, \psi_R(\mathbf{r}) + i \sin Mt\, \psi_L(\mathbf{r})] e^{-iE_0 t} \qquad (13)$$

which starts with a right-hand-side state at t = 0.

The linear combinations of the solutions, equation (12) and equation (13), are also good solutions of the time-dependent Schrodinger equation, equation (2). For example, there is a state symmetric with respect to the median plane:

$$\begin{aligned} \Psi_g(\mathbf{r}, t) &= [\Psi_1 + \Psi_2] \\ &= [\psi_L(\mathbf{r}) + \psi_R(\mathbf{r})] e^{-i[E_0 + M]t}, \end{aligned} \qquad (14)$$

as well as an antisymmetric state:

$$\begin{aligned} \Psi_u(\mathbf{r}, t) &= [\Psi_1 - \Psi_2] \\ &= [\psi_L(\mathbf{r}) - \psi_R(\mathbf{r})] e^{-i[E_0 - M]t}. \end{aligned} \qquad (15)$$

Apparently, these solutions represent **stationary states** of equation (2) with energy eigenvalues $[E_o + M]$, and $[E_o - M]$, respectively. Because both E_o and M are negative, the symmetric state has a lower energy, which means an attractive force.

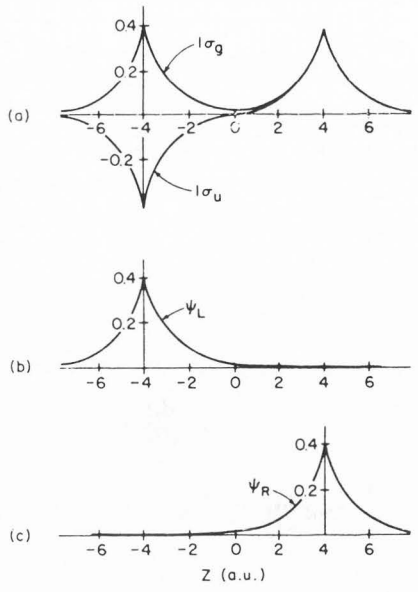

Figure 4. Wavefunctions of the hydrogen molecular ion. **(a)** The exact wavefunctions of the hydrogen molecular ion. Two lowest states are shown. The two exact solutions can be considered as symmetric and antisymmetric linear combinations of the solutions of the left-hand-side and right-hand-side problems, **(b)** and **(c)**, defined by potential curves in Figure 3. For brevity, the normalization constant is omitted.

The above discussion is a quantitative formulation of the concept of **resonance** introduced by Heisenberg (1926) for treating many body problems in quantum mechanics. Heisenberg illustrated this concept with a classical mechanical model (see Pauling and Wilson, 1935): two similar pendulums connected by a weak spring. According to this classical analogy, the meaning of equation (12) is as follows: At t < 0, the right-hand-side pendulum is held still, and the left-hand-side pendulum is set to oscillate with a frequency $|E_o|/h$. At t = 0, the right-hand-side pendulum is released. Because of the coupling through the weak spring, the left-hand-side pendulum gradually ceases to oscillate, transferring its energy to the right-hand-side pendulum, which gradually increases its amplitude of oscillation. At $t = \pi/|M|$, the right-hand-side pendulum reaches the maximum amplitude, and the left-hand-side pendulum stops. Then, the process reverses. This mechanical system has two normal modes, with the two pendulums oscillating in the opposite directions or in the same direction, with frequencies $[E_o + M]/h$, and $[E_o - M]/h$, respectively. These two normal modes correspond to the symmetric and antisymmetric states of the hydrogen molecular ion, respectively, as shown in Figure 4. The two curves in part (a) of Figure 4 are the exact solutions of the two low-energy solutions of the $H2^+$ problem.

To a good approximation, these solutions can be represented by the symmetric and antisymmetric superpositions of the distorted hydrogen wavefunctions, as shown in parts (c) and (d) of Figure 4. These wavefunctions are defined by the left-hand-side and right-hand-side potentials (Figure 3). The total coupling energy is the sum of the van der Waals energy, equation (1), and the resonance energy, equation (11). For the $1\sigma_g$ state, it is:

$$\Delta E(1\sigma_g) = -\frac{9}{4R^4} - \frac{2}{e} Re^{-R}, \tag{16}$$

and for the $1\sigma_s$ state,

$$\Delta E(1\sigma_u) = -\frac{9}{4R^4} + \frac{2}{e} Re^{-R}. \tag{17}$$

Repulsive force

As shown in Figure 2, as the proton-proton separation becomes even smaller, the picture of resonance becomes obscured, and the proton-proton repulsion is no longer screened by the electron. Slater (1963) shows that the Morse curve matches the exact potential curve with a high accuracy:

$$f = C\left[e^{-2\kappa(s-s_0)} - e^{-\kappa(s-s_0)}\right], \tag{18}$$

where s_0 is the equilibrium point, and C is a constant.

Force and tunneling conductance

As we have shown in the **Resonance energy** section, the transition matrix element, equation (10), has two meanings. First, it determines the binding energy between the two interacting systems. The force is the rate of change of the binding energy with respect to distance, therefore,

$$F = -\frac{\partial |M|}{\partial z}. \tag{19}$$

Next, the tunneling conductance can be calculated from the tunneling matrix element through the Fermi golden rule (Bardeen, 1960; Duke, 1969). For metals, the variation of the tunneling matrix element M and the density of states ρ over the valence band is small in comparison with their absolute values. A simple relation between the force and the tunneling current can be established. Assuming that the width of the valence band ϵ for the tip and the sample are approximately equal, the density of states is $\rho = \epsilon^{-1}$ for both. The tunneling conductance is then

$$G = \frac{(2\pi)^2}{R_K \epsilon^2} |M|^2, \tag{20}$$

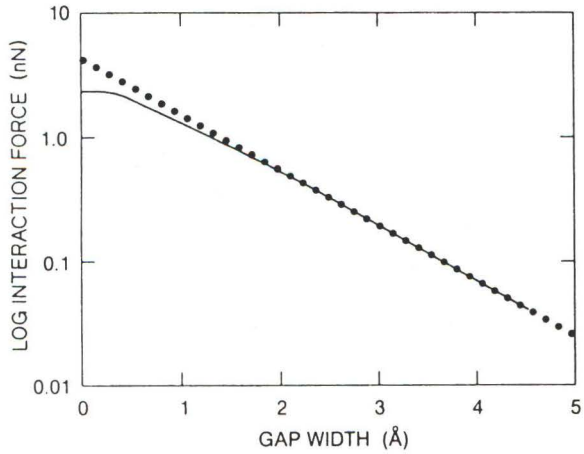

Figure 5. Comparison of the theoretical and measured forces in STM. The solid curve is the measured dependence of the attractive force by Dürig *et al.* (1988). The dotted curve represents equation (22). Parameters used for curve fitting: work function $\phi = 4$ eV, width of valance band $\epsilon = 5$ eV, and $f \approx 1$. The origin of the abscissa corresponds to $G = 10^{-5}\ \Omega^{-1}$. At very short tip-sample distances, the repulsive force occurs, which reduces the net attractive force. After Dürig *et al.* (1988).

---

where $R_\kappa = h/e^2 = 25812.8\ \Omega$ is von Klitzing's constant. Experiments have shown that over the entire range of STM operation, the tunneling conductance varies exponentially with tip-sample distance, $G \propto \exp(-2\kappa z)$, where $\kappa = (2m_e\phi)^{1/2}/\hbar$ is the decay constant of the surface wavefunction, and ϕ is the workfunction of the material. Combining equation (19) and equation (20), we obtain

$$F = -\frac{\kappa \epsilon}{2\pi} \sqrt{GR_K}. \tag{21}$$

The force between a tip and a flat depends on the shape of the tip. By defining a dimensionless number of the order of unity, the shape factor f, the force is related to the tunneling conductance by

$$F = -f\kappa\epsilon\sqrt{GR_K}. \tag{22}$$

For tips with a paraboloidal end, $f = 2/\pi \approx 0.637$; and for tips with a conical end, $f = 4/\pi \approx 1.27$. Figure 5 shows a comparison of equation (22) with experimental observations.

STM Imaging as a Chemical Process

In the previous section, we have shown that the tunneling process in STM is a charge transfer process

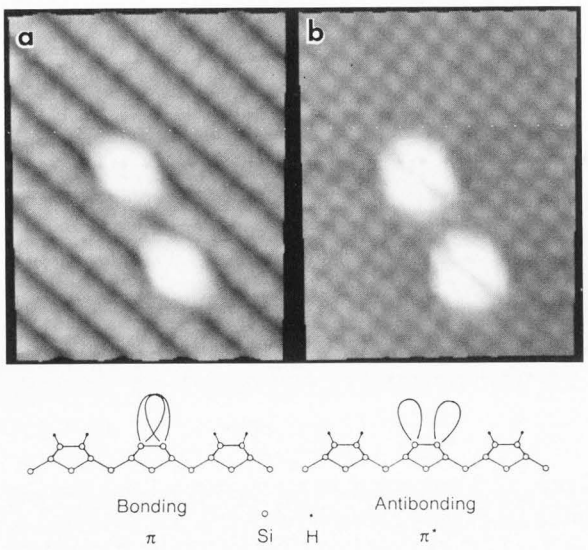

Figure 6. Observation of individual π bonds by STM. On a nascent Si(100) surface, every surface Si atom has p_z-type dangling bond with it. By saturating the Si(100) surface with hydrogen, all the p_z-type dangling bonds are capped with a hydrogen atom. By heating the hydrogen-saturated Si(100) surface carefully, a small fraction of the hydrogen atoms are desorbed. The p_z-type dangling bonds on the Si atoms are paired to form π bonds. (**a**) The filled π state which has a symmetric structure. This is a typical example of the covalent chemical bond which binds atoms together to form molecules and solids. (**b**) Empty π^* state which as expected exhibits a node between the dimer atoms. (**c**) Schematics of these orbitals. After Boland (1991).

---

between the electronic states of the tip and the electronic states of the sample. Consider a simple case that the electronic states on each sample atom are approximately mutually independent. The tunneling process is determined by the charge transfer process between the sample states and tip electronic state. When a tip state approaches the sample, the tip electronic state forms a partial chemical bond with an atomic state on the sample, thus generating a tunneling current. When the tip moves horizontally, it breaks the partial chemical bond with that atom. Then, the tip state forms a partial chemical bond with the next atom. The condition of keeping the tunneling conductance constant means keeping the overlap of the tip electronic state and the sample electronic state constant. The image corrugation is then determined jointly by the tip electronic states and the sample electronic states. For a given sample surface, the corrugation of the image is determined by the "sharpness" of the tip state.

In the following, we discuss the roles of sample electronic states and the tip electronic states.

Role of sample electronic states

One of the best illustrations of the importance of the sample electronic states in the STM image is the direct observation of individual chemical bonds using the STM. In the following, we will describe the experimental observations of Boland (1991), as shown in Figure 6.

The experiment was performed on the Si(100) surface. On the bare Si(100) surface, each Si atom has a p_z-type dangling bond protruding into the vacuum. By exposing the Si(100) surface with hydrogen, all dangling bonds are capped with hydrogen atoms. By mildly heating up the Si sample, some of the hydrogen atoms are evaporated, and the dangling bonds on these Si atoms reappear. Boland (1991) found that the dangling bonds always form pairs. The STM topographic images of those pairs look differently at different biases. At a negative bias, when the occupied states are imaged, a pair appears as a single protrusion. At a positive bias, when the unoccupied states are imaged, a pair appears as a double peak, with a seam in the middle. This is a manifestation of the individual chemical bonds in real space. At a negative bias, the STM images the bonding state, or the π-orbital. At a positive bias, the STM images the antibonding state, or the π^*-orbital.

Obviously, the STM images of the individual chemical bonds cannot be interpreted by a single quantity of the sample surface, such as the Fermi-level local density of states (LDOS). Actually, in this case, the Fermi-level LDOS of the sample surface is almost zero, and the images at different biases are very different; the STM images can only be explained by the electronic structure of the sample surface off the Fermi level, i.e., the sample electronic states either below the Fermi level or above the Fermi level.

Role of tip electronic states

We have shown in the previous subsection that the atom-resolved STM images are related to the atomic electronic states of the sample surface. Because the sample and the tip play an equal role in determining the tunneling current, a logical consequence is that the atomic electronic states of the tip should be equally important.

The necessary condition to obtain atomic resolution is that the tip ends with a single atom. The electronic states of the apex atom depends not only on the nature of this atom, but also the configuration of surrounding atoms. This explains the often-observed fact that for a given sample surface, there are many different STM images. Because the electronic states of the apex atom still have atomic characters, its electronic states can be described in terms of spherical harmonics. In other words, the electronic states of the tip atom still can be described by quantum numbers l and m, and its energy

level, although some mixing of states and the shift as well as the broadening of the energy level are always present. For example, in a free atom, because of the spherical symmetry, electronic states with different magnetic quantum number m are degenerate. For a tip atom, because of the strong interaction with the surrounding atoms, the electronic states with different m usually have different energy levels.

A schematic of the wavefunctions of different atomic states is shown in Figure 7.

The s-state ($l = 0$, $m = 0$) dominates the electron density of alkali metal atoms (such as Na) and alkali-earth metal atoms (such as Ca) near the Fermi level. As shown in Figure 7, the s-state is the bluntest of all atomic electronic states.

The p-states are the dominate atomic states near the Fermi level for many commonly used materials such as C, Si, and Ge. The p_z ($l = 1$, $m = 0$) is omnipresent on the surfaces of graphite, germanium, and silicon. As shown in Figure 7, the p_z tip state is much sharper than the s-wave state. This provides an interpretation of the observed atomic resolution in STM (Demuth *et al.* 1988).

The STM tips are made of d-band metals, such as W, Pt, and Ir. The different d-states dominate the electron density near the Fermi level. It was known for decades that on W(001) and Mo(001) surfaces, the d_{z^2} state dominates the surface electron density near the Fermi level (Weng *et al.*, 1978; Posternak *et al.* 1980). On W clusters, there are also d_{z^2} states near the Fermi level (Ohnishi and Tsukada, 1989). As shown in Figure 7, the d_{z^2} tip state is the sharpest. On metal surfaces, the atomic corrugation generated by a d_{z^2} tip state can be 20 times greater than that from an s-wave tip state (Wintterlin *et al.* 1989; Chen, 1990).

Because of the interaction of the tip atom with the tip stem, the energy levels of the $m \neq 0$ tip states are split from that of the $m = 0$ states. Depending on the actual condition, either a $m = 0$ state or the $m \neq 0$ states can dominate the electron density near the Fermi level. If the tip has an axial symmetry, the state with same $|m|$ are degenerate. If the tip does not have an axial symmetry, the states with $+m$ and $-m$ might split in energy levels. In the first case, the tip electron density appears as a ring, with a hole at x = 0 and y = 0. On metal surfaces, the STM image should be inverted, that is, each atomic site on the sample surface would be a depression instead of a protrusion in the topographic STM image. Such inverted images were often observed (Barth *et al.* 1990).

The presence of different d states on a d-band metal tip ending with a single atom is demonstrated experimentally by Binh *et al.* (1992) using field emission spectroscopy (FES). Their observations indicated that the

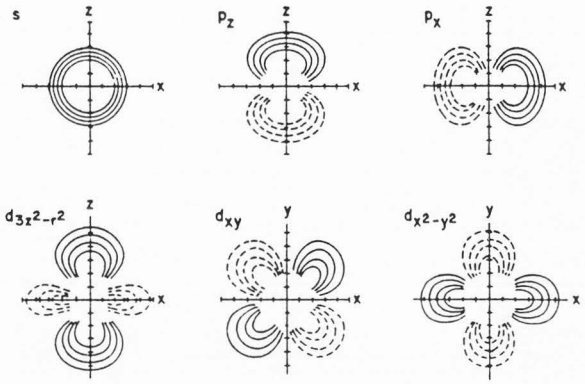

Figure 7. Charge density contours of different atomic states. The regions with dashed-curve contours have opposite phases in the wavefunction from those with solid-curve contours.

FES of the tips ending with a single atom are dramatically different from a free-electron-metal tip, and have many different forms. For a free-electron-metal tip, the FES has a clear edge near the Fermi level, and the shape of the spectrum almost does not change with applied voltage. For tips ending with a single atom, the FES become very different, as shown in Figure 8. The edge at the Fermi level disappears. Instead, several prominent peaks emerge. The positions of these peaks change dramatically with the details of tip structure, and varies with applied voltage (Binh *et al.*, 1992).

The one-sided view that the STM image only depends on the sample surface, and does not depend on the tip electronic state, cannot explain the observed atomic resolution in STM, and cannot explain the large variety of different STM images of the same sample surface (see Figure 9). As shown by Tersoff and Hamann (1985), on a large scale, if the atomic details of the surface is neglected, and the tip is sharp enough, then the one-sided view has some truth in it. During a scan, the same tip state encounters a large number of sample states. The large-scale features of the STM images are determined by the sample only. This is analogous to some ballets such as Peter Tchaikovski's *The Swan Lake* or Frédéric Chopin's *Les Sylphides*. In these cases, *le danseur* performs the ballet with *les cygnes* or *les sylphides*, which determine the spectacle on a large scale. Nevertheless, the performance of the ballet is by no means independent of the choice of *le danseur*. By choosing Michael Bareshnikov, Michael Tyson, or chimpanzee Michael as *le danseur*, the ballet would look differently. The STM experimentalists take a lot of time trying to invite Michael Bareshnikov as *le danseur*, and probably never willing to publish an image (that is, to show a ballet) with Michael Tyson or chimpanzee Michael as *le danseur*. Although viewing from a kilo-

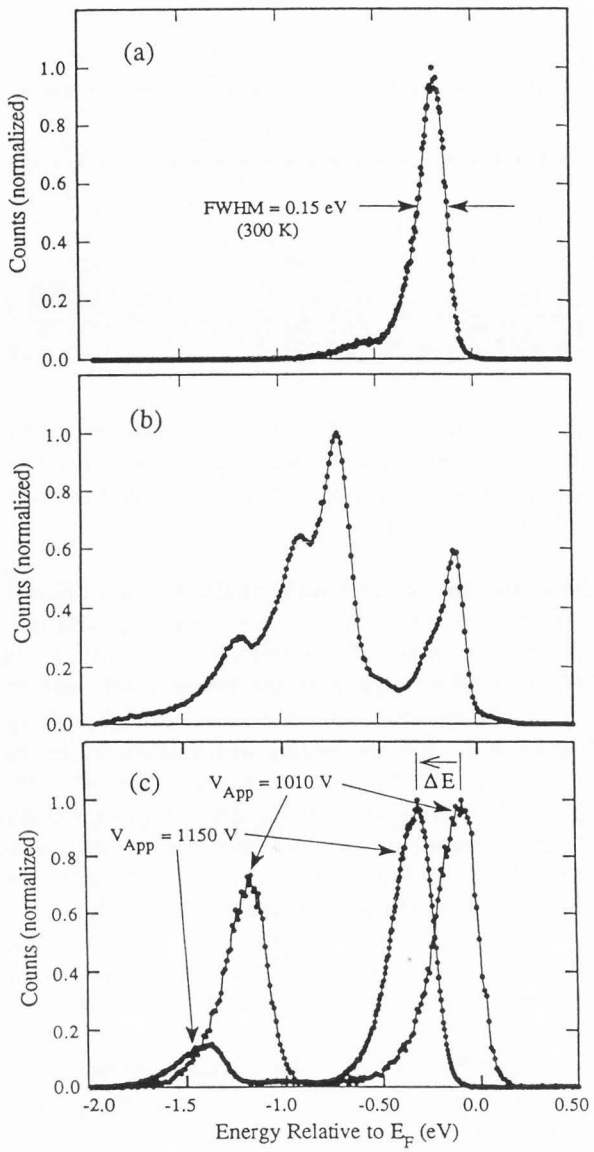

Figure 8. Experimental field-emission spectra of a W tip with a single protruded atom. The FES of tips with single-atom protrusion depends dramatically on the details of the atomic structure near the apex. These spectra consist of well-separated peaks, whose positions depends on the applied voltage. After Garcia *et al.* (1993).

---

meter away, Michael Bareshnikov, Michael Tyson, or chimpanzee Michael, would look the same (that is, a little dot), it does not mean that they would perform *The Swan Lake* or *Les Sylphides* equally well. In fact, for the important role of tip electronic states in STM images with atomic resolution, Tersoff and Lang (1990) has made a lucid illustration. They showed that the STM images from different tip atoms, Na, Ca, Si, Mo, and C, are dramatically different. When a Na or a Ca atom

Figure 9 (on the facing page). STM images of 4Hb-TaS_2 at 4.2 K. These images were taken during a period of about 2 hours on the same area of the surface under identical tunneling conditions (current = 2.2 nA, voltage = 25 mV). These images demonstrate the role of tip electronic states on the STM images. After Coleman *et al.* (1990).

---

is the tip atom, the STM images are similar to the prediction of the *s*-wave tip model (Tersoff and Hamann, 1985). Nevertheless, real tips are neither Na or Ca, but rather transition metals, probably contaminated with atoms from the surface (for example, Si and C are common sample materials). For a Si-atom tip, the *p* state dominates the Fermi-level LDOS of the tip. For a Mo-atom tip, while the *p* contribution is reduced, this is more than compensated by the large contribution from states of *d* like symmetry. The STM images from a Si, C, or Mo tip, as predicted by Tersoff and Lang (1990), are dramatically different from the images predicted by the *s*-wave-tip model.

Tip-Induced Chemistry

As we have shown, in the normal operation of an STM, there is a partial chemical bonding between the tip state and the sample state. One would expect that the tip would be able to play an active role in inducing chemical reactions on the sample or with the sample. Two types of chemical reactions are reported. The first one is the chemical reactions on the sample induced by the tip. The second one is the transfer of atoms between the tip and the sample. We will describe examples to each cases, both were performed on Si(111)-7x7 surfaces.

Tip-induced surface chemical reaction

Lyo and Avouris (1990) showed that the tip can remove the OH or H fragments from a Si surface. Their experiment is as follows:

The STM image of the Si(111)-7x7 surface shows that there are dangling bonds on the top-layer adatoms. Exposing this surface to water vapor leads to the elimination of a large number of dangling bonds, as shown in Figure 10a. Experimental evidence showed that the water molecule dissociated to become OH and H fragments, both can tie up with the dangling bonds. By scanning the tip at a bias +3 V at the sample, the image changed. A subsequent image taken at +2 V shows that many of the dangling bonds reappear. Obviously, during the scan at +3 V, many of the OH or H are removed from the Si sites by the chemical actions of electronic states of the tip (see Figure 10b).

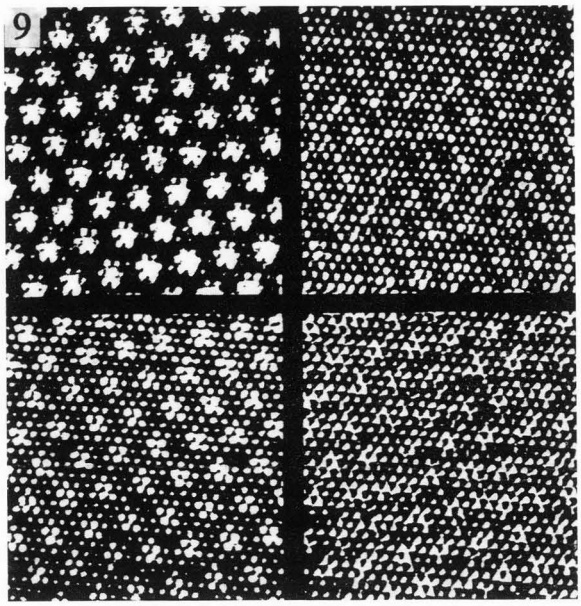

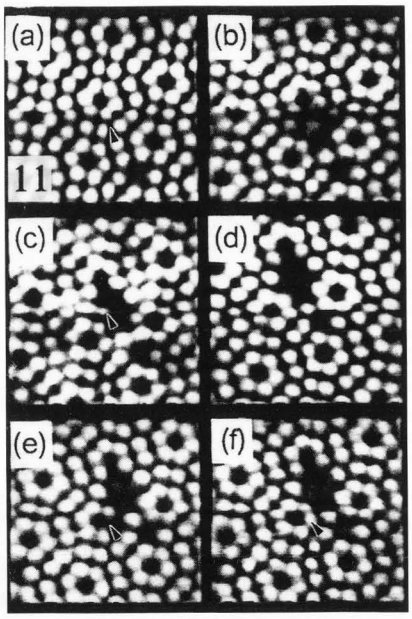

Figure 11. Exchange atoms by the STM tip. The series of experiments was performed on Si(111)-7X7 surface at room temperature in ultra high vacuum. (**a**) The tip is placed at ≈ 1 Å from electronic contact over the site indicated by the arrow. (**b**) A 1.0 V pulse removes 3 atoms leaving the fourth under the tip. (**c**) The first attempt to remove this atom leads to its migration to the left (see arrow) and bonding as a center adatom. (**d**) A second pulse removes this fourth atom. (**e**) A new comer-atom is removed and in (**f**) it is placed back to its original position. After Lyo and Avouris (1991).

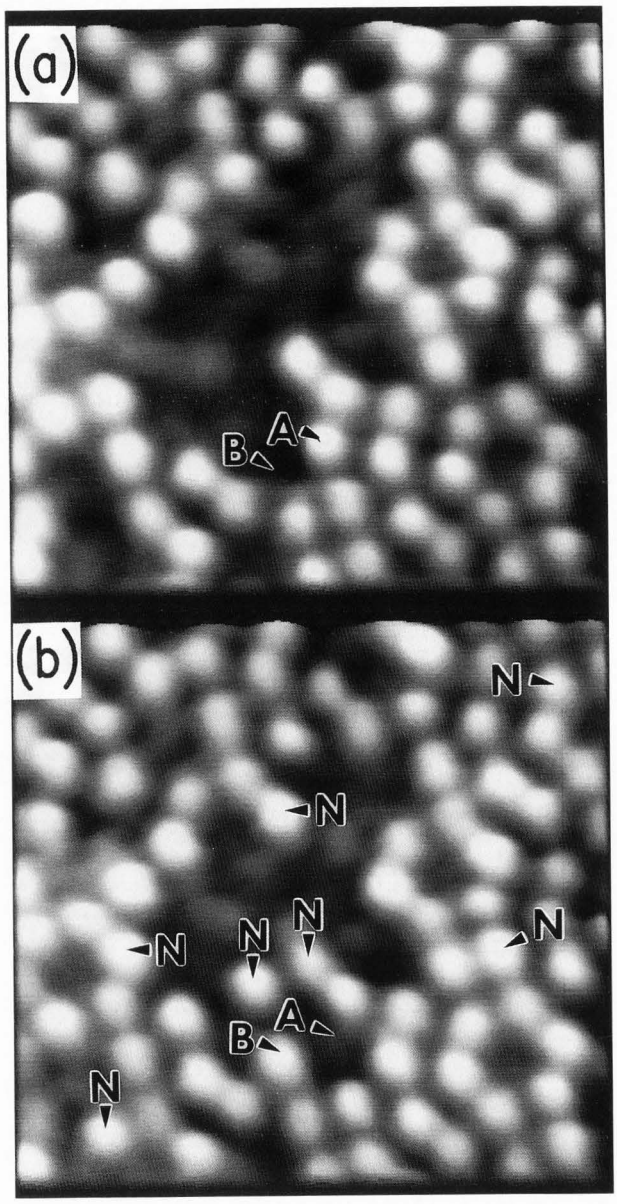

Figure 10. Tip-induced desorption of OH group on Si(111)-7x7. (**a**) STM topograph of a 72x72 $Å^2$ area of H_2O-exposed Si surface. Sample bias +2 V. (**b**) After it has been scanned with sample voltage +3 V, on many of the reacted sites, the dangling bonds reappeared, as denoted by N. Moreover, it appears that the adsorbate on site B in (a) may have moved to site A in (b). After Lyo and Avouris (1990).

Exchanging atoms between tip and sample

Another experiment is also demonstrated by Lyo and Avouris (1991), see Figure 11. At room temperature, on Si(111)-7x7 surfaces, by applying electrical pulses between the tip and the sample, individual Si

atoms can be transferred from the sample to the tip and *vice versa*.

Conclusions

In summary, we have presented a chemical perspective for scanning tunneling microscopy. The origin of both the tunneling current and the chemical bond is a charge transfer process on an atomic scale. This process is based on the overlap of the wavefunctions of both parties. Thus, the imaging process of STM can be considered as a sequence of local bond forming and bond rupturing. This point of view provides a heuristic interpretation of the observed atomic resolution as well as the tip-induced chemical reactions.

References

Avouris Ph (1990) Atom-resolved surface chemistry using the scanning tunneling microscope. J. Phys. Chem. **94**, 2246-2256.

Baratoff A (1984) Theory of scanning tunneling microscopy - Methods and approximations. Physica (Amsterdam) **127B**, 3-150.

Bardeen J (1960). Tunneling from a many-body point of view. Phys. Rev. Lett. **6**, 57-59.

Barth JV, Burne H, Ertl G, Behm RJ (1990) Scanning tunneling microscopy observations on the reconstructed Au(111) surface: Atomic structure, long-range superstructure, rotational domains, and surface defects. Phys. Rev. **B 42**, 9307-9318.

Binh VT, Purcell ST, Garcia N, Doglini J (1992) Field emission spectroscopy of single-atom tips. Phys. Rev. Lett. **69**, 2527-2530.

Binnig G, Rohrer H (1982) Scanning tunneling microscopy. Helv. Phys. Acta. **55**, 726-735.

Binnig G, Rohrer H (1986). Scanning tunneling microscopy. IBM J. Res. Develop. **30**, 355.

Binnig G, Quate CF, Gerber Ch (1986) Atomic force microscope. Phys. Rev. Lett. **56**, 930-933.

Boland JJ (1991) Evidence of pairing and its role in the recombinative desorption of hydrogen from the Si(100)-2x1 structure. Phys. Rev. Lett. **67**, 1539-1542.

Chen CJ (1990) Origin of atomic resolution on metals in scanning tunneling microscopy. Phys. Rev. Lett. **65**, 448-451.

Chen CJ (1991a) Microscopic view of scanning tunneling microscopy. J. Vac. Sci. Technol. **A 9**, 44-50.

Chen CJ (1991b) Attractive atomic force as a tunneling phenomenon. J. Phys.: Cond. Matter **3**, 1227-1245.

Chen CJ (1993) Introduction to Scanning Tunneling Microscopy. Oxford University Press.

Coleman RV, Giambattista B, Hansma PK, Johnson A, McNairy WW, Slough CG (1988) Scanning tunneling microscopy of charge-density waves in transition metal chalcogenides. Adv. Phys. **37**, 559-644.

Dalton J (1808) A New System of Chemical Philosophy. Reprinted by Philosophical Library, New York, 1964.

Demuth JE, Koehler U, Hamers RJ (1988) The STM learning curve and where it may take us. J. Microsc. **151**, 289-302.

Duke CB (1969) Tunneling in Solids, Academic Press, New York.

Dürig U, Züger O, Pohl DW (1988). Force sensing in scanning tunneling microscopy: Observation of adhesion forces on clean metal surfaces. J. Microsc. **152**, 259-267.

Flores F, Martin-Rodeno A, Goldberg EC, Duran JC (1988) Molecular orbital theory and tunneling currents. Nuovo Cimento **10 D**, 303-311.

Garcia N, Binh VT, Purcell ST (1993) Structurally induced FEES from nanotips: Implications for scanning tunneling spectroscopy. Surf. Sci. Lett. **293**, L884-L887.

Hamers RJ (1989) Atomic-resolution surface spectroscopy with the scanning tunneling microscope. Ann. Rev. Phys. Chem. **40**, 531-559.

Heisenberg W (1926) Mehrkorperproblem und Resonanz in der Quantunmechanik (Many-body problems and resonance in quantum mechanics) Z. Phys. **38**, 411-426.

Herring C (1962) Critique of the Heitle-London method of calculating spin couplings at large distances. Rev. Mod. Phys. **34**, 631-645.

Holstein T (1955) Charge-exchange interaction between ions and parent atoms, Westinghouse Research Report 60-94698-3-R9. Available from Westinghouse Sci. and Tech. Ctr., Pittsburgh, PA 15235, USA.

Landau LD, Lifshitz LM (1977) Quantum Mechanics, 3rd Edition. Pergamon Press, Oxford. p. 312.

Lyo IW, Avouris Ph (1990) Atomic scale processes induced by the scanning tunneling microscope. J. Chem. Phys. **93**, 4479-4480.

Lyo IW, Avouris Ph (1991) Field induced nanometer to atomic scale manipulation of silicon surfaces with the STM. Science **253**, 173-176.

Ohnishi S, Tsukada M (1989) Molecule orbital theory for the scanning tunneling microscopy. Solid State Commun. **71**, 391-394.

Pauling L (1977) The Nature of the Chemical Bond, 3rd Edition. Cornell University Press, Ithaca, NY.

Pauling L, Wilson EB (1935) Introduction to Quantum Mechanics. McGraw-Hill, New York.

Posternak M, Krakauer H, Freeman AJ, Koelling DD (1980) Self-consistent electronic structure of surfaces: Surface states and surface resonances on W(001). Phys. Rev. **B 21**, 5601-5612.

Slater JC (1963) Quantum Theory of Molecules and Solids, Vol. 1. McGraw-Hill, New York.

Tersoff J, Hamann DR (1985) Theory of scanning tunneling microscope. Phys. Rev. **B 31**, 805-808.

Tersoff J, Lang ND (1990) Tip-dependent corrugation of graphite in scanning tunneling microscopy. Phys. Rev. Lett. **65**, 1132-1135.

Weng SL, Plummer EW, Gustafsson T (1978) Experimental and theoretical study of the surface resonances on the (100) faces of W and Mo. Phys. Rev. **B 18**, 1718-1740.

Wintterlin J, Wiechers J, Brune H, Gritsch T, Hofer H, Behm RJ (1989). Atomic-resolution imaging of close-packed metal surfaces by scanning tunneling microscopy. Phys. Rev. Lett. **62**, 59-62.

Discussion with Reviewers

M. Tsukada: The atom-atom interaction energy would be in proportion to $|M|$ for the exact resonance case, as discussed here. But for off-resonant cases, for instance, $(Li\text{-}H)^+$ system, the interaction energy might be proportional to $|M|^2$, and such a case seem to be more realistic model of tip-surface system. On the other hand, I believe, for a realistic continuum model of tip-surface electronic states, equation (19) is no more valid because of other types of interactions as discussed by Lifshitz [Sov. Phys. JETP **2**, 73 (1956)]. In these interactions, the overlap of tip and surface wave-function is not necessary.

Author: In the case of metal-metal tunneling, the strict resonance condition is always valid. In fact, even in the classical paper of Bardeen (1960), the resonance condition $E_i = E_j$ is explicitly stated. Therefore, the resonance energy should be proportional to $|M|$. If at least one of the electrodes is not metallic, the resonance condition is no longer valid. The exchange energy is thus proportional to the matrix element of the second-order perturbation theory. There is no direct tunneling current. The indirect tunneling current is determined by the first Fermi golden rule, which is proportional to the square of the matrix element of the second-order perturbation theory. The proportionality relation between the resonance energy and the square of the tunneling conductance is still valid. However, the effect is much more feeble, usually smaller than the van der Waals force. The Lifshitz theory is about the van der Waals force, which exists even between insulators. The experimental verification of the Lifshitz theory is always performed by a pair of good insulators, such as mica. Of course, in the discussion of atomic force microscopy of insulators, the Lifshitz theory is valid, and there is no resonance energy. However, for two pieces of metals within the distance of tunneling, the adhesive energy (or the exchange interaction) is always much larger than the van der Waals energy, which is the circumstance discussed in this paper.

V.T. Binh: The importance of the electronic states of both the tip and the sample was highlighted in this review paper. The tip electronic states are a function of its nature and geometry. Could the author speculate on the best type of tip to be used in each of the different functions he has enumerated (for imaging metals or semiconductor surfaces, for tip-induced chemistry, structure manipulation, ...), thus as a guide to experimentalists working in STM.

Author: Although the importance and effect of tip electronic states are well recognized, the nature of the tip electronic structure together with its specific effect on images and tip-induced phenomena is one of the central but unresolved problems in the field of STM. Actually, the ongoing studies of Dr. Binh and his collaborators on tip electronic structures may reveal crucial evidences for resolving this problem. I hope that this problem can be fully clarified in the near future.

S.M. Lindsay: Julian Chen's lucid review offers a valuable perspective on STM: that it can be viewed as a process of chemical "bond" formation between tip and substrate. It is a valuable perspective which helps to embrace some of the true complexities of STM image formation while making it much easier to exploit the vast body of phenomenological data that the chemists can bring to bear on this problem. Chen has expounded this view in a brilliant series of papers and used it to draw the whole field together in what will be the definitive book on STM for years to come (Chen, 1993). I would like to add two points to this review:

a) These considerations apply to the atomic force microscope also. This instrument operates (in the "contact mode") by forming bonds between a probing stylus and a substrate. This is illustrated rather dramatically by the controlling influence of the **adhesion** force on the resolution and apparent height of small molecules imaged with an AFM (although the tip is nominally an insulator, it can contain surface moieties that "react" with the substrate, producing adhesion) [{Yang J, Shao Z (1993) The effect of probe force on the resolution of atomic force microscopy of DNA. Ultramicroscopy, **50**: 157-170} and {Lyubchenko YL, Oden PI, Lampner D, Lindsay SM, Dunker KA (1993) Atomic force microscopy of DNA and bacteriophage in air, water and propanol: The role of adhesion forces. Nucleic Acids Research **21**: 1117-1123}].

b) The modified transfer Hamiltonian approach is both useful and pedagogical valuable. It is, however, a perturbation theory and will not be valid if the coupling

is very strong. In the case of molecular adsorbates, we have gained some insight using a tight binding model [Lindsay SM, Sankey OF, Li Y, Herbst C (1990) Pressure and resonance effects in scanning tunneling microscopy of molecular adsorbates. J. Phys. Chem. **94**: 4655-4660].

Author: Thank you for your comments.